Erosion of Tungsten Marker Layers in W7-X

M. Mayer[a], M. Balden[a], S. Brezinsek[b], C.P. Dhard[c], S. Elgeti[a], D. Fajardo[a], J. Fellinger[c], M. Guitart Corominas[a,d], P. Hiret[a], M. Kandler[a,d], D. Loesser[e], A. Lumsdaine[f], D. Naujoks[c], H. Neilson[e], R. Neu[a,d], J. Oelmann[b], C. Ruset[g], J.-H. Schmidt-Dencker[a], and W7-X Team

[a]*Max-Planck-Institut für Plasmaphysik, Garching, Germany*
[b]*Forschungszentrum Jülich GmbH, Jülich, Germany*
[c]*Max-Planck-Institut für Plasmaphysik, Greifswald, Germany*
[d]*Technische Universität München, Garching, Germany*
[e]*Princeton Plasma Physics Laboratory, Princeton, USA*
[f]*Oak Ridge National Laboratory, Oak Ridge, USA*
[g]*National Institute for Laser, Plasma and Radiation Physics, Bucharest, Romania*

Abstract

In order to get first insight into net tungsten erosion in W7-X tungsten (W) marker layers were exposed during the operational phase OP 1.2b at one position of the Test Divertor Unit (TDU), at 21 different positions of the inner heat shield, and at two scraper elements. The maximum tungsten erosion rate at the TDU strike line was 0.13 nm/s averaged over the whole campaign. The erosion was inhomogeneous on a microscopic scale, with higher erosion on ridges of the rough surface inclined towards the plasma and deposition of hydrocarbon layers in the recessed areas of the rough surface. The W erosion at the inner heat shield was below the detection limit of $3 – 6 \times 10^{12}$ W-atoms/cm^{2}s, and all inner heat shield tiles were covered with a thin B/C/O layer with thicknesses in the range $2 \times 10^{17} – 10^{18}$ B + C atoms/cm^2 (about 20 – 100 nm B + C). W-erosion of the marker layers on the scraper elements was also below the detection limit.

1. Introduction

The Wendelstein 7-X (W7-X) experiment [1, 2, 3, 4] is currently, besides the Large Helical Device (LHD), the largest operating stellarator in the world. It is an advanced stellarator with superconducting coils, a plasma volume of 30 m^3 and a large radius of 5.5 m. During the second operational phase (OP 1.2) in the years 2017 – 2018 an inertially cooled divertor, the so-called Test Divertor Unit (TDU) [5, 6], baffles, an inner heat shield, wall panels and poloidal as well as toroidal closures were installed. Most plasma-facing components (PFCs) are made of fine-grain graphite, the outer wall consists mostly of stainless steel components. The TDU implements the island divertor concept [7], where chains of islands at the plasma edge provide multiple x-points and the plasma intersects the divertor plates at some distance from the closed flux surfaces. The successful application of this concept was already demonstrated at the antecessor experiment W7-AS [8]. The TDU has the same plasma-facing contour as the water-cooled steady-state divertor equipped with carbon-fiber-composite PFCs that is currently being installed.

During the first operational phase with TDU (OP 1.2a) in 2017 wall conditioning was performed using glow discharge cleaning (GDC) without boronizations. A very high erosion of carbon was observed at the TDU strike line positions [9] due to high levels of oxygen, which has a chemical erosion yield close to one

by formation of CO and CO_2. Erosion of carbon by oxygen subsequently also resulted in high carbon levels in the plasma. The oxygen originated from outgassing of water from carbon components [10]. During the whole operational phase OP 1.2a in total 48±14 g carbon were eroded from the TDU [9].

In the succeeding operational phase OP 1.2b in the year 2018 three boronizations were applied. This resulted in a strong decrease of the oxygen and carbon concentrations in the plasma [11, 12]: After the third boronization the oxygen level was about two orders of magnitude lower compared to the pre-boronization values, while Z_{eff} decreased from 4.5 to values close to 1.2 in reference discharges. This decrease of the low-Z impurity concentration significantly extended the operational window of W7-X towards higher plasma densities: the line-integrated electron density increased from 4×10^{19} m^{-2} to more than 1×10^{20} m^{-2} [11]. This decrease of impurities was also associated with a substantial decrease of the observed carbon erosion rates at the TDU strike line positions by a factor of more than five [10, 13]. Nevertheless, despite the observed decrease of the carbon erosion rate due to decreased oxygen content, the carbon erosion at the TDU was still not small, and during OP 1.2b in total 20±6 g carbon were eroded at the TDU [13].

The eroded carbon was partly redeposited inside the machine, and thicker redeposited layers consisting mostly from carbon with hydrogen, oxygen and boron (the latter mostly at the surface) and with thicknesses ranging from several 100 nm to more than 10 μm were found especially on some baffle tiles [14]. Some of these layers already started to flake off. This raises concern for the foreseen long-pulse operation with planned pulse durations up to 1800 s, especially in the light of the experience gained during the DITS campaign [15] in the Tore Supra tokamak: During that campaign identical discharges were repeated for 5 plasma hours and resulted in the formation of thick redeposited layers at various places inside the machine. The flaking of these layers hindered plasma operation considerably and finally forced a change of the discharge scenario [15].

A potential solution to overcome the relatively large erosion and succeeding redeposition of carbon is the use of tungsten as plasma-facing material [16]: At detached plasma conditions and low plasma impurity contents the erosion of tungsten by hydrogen ions is extremely small, and tungsten is successfully used in a number of tokamaks worldwide, such as ASDEX Upgrade [17], JET [18], WEST [19] and EAST [20]. However, the use of high-Z materials in stellarators is more challenging due to the higher contribution of neoclassical transport in stellarators compared to tokamaks. As was already observed experimentally, neoclassical transport can result in accumulation of high-Z impurities in the plasma [21]. The neoclassical inward-drift is counterbalanced by turbulent transport, which plays also an important role in W7-X [22]. First results hint to the fact that impurity accumulation might be not a problem during turbulence-dominated discharges. However, it was shown by impurity injection experiments that impurity accumulation can occur during turbulence-suppressed phases: This can be a challenge for future long pulse operation [22].

Due to this potential problem of high-Z impurity accumulation PFCs with high-Z elements have to be introduced carefully in W7-X. This paper describes first experimental observations on tungsten erosion at the TDU, the inner heat shield, and on scraper elements.

2. Experimental

2.1 Plasma operation

The operational phase OP 1.2b lasted from July to October 2018 and had a total plasma time of 9054 s. Most discharges (4809 s, 53.1% of the plasma time) were in Standard configuration, the remaining discharges were in Low Iota (1180 s), High Iota (1673 s) or High Mirror (1392 s) configuration [10, Table II]. All configurations have their strike lines on different areas of the TDU [6]. All discharges were in hydrogen, deuterium discharges were not performed. While all possible types of divertor plasmas were performed, more exotic configurations were very limited in time. The dominant plasma scenario had a pulse duration of about 10 s, medium ECR heating power of 3 to 4 MW, and attached divertor conditions.

The Standard configuration has its strike line on the horizontal target modules TM1h to TM4h and the vertical target modules TM1v to TM3v, see e.g. [6] for details. Divertor heat loads reached values up to 8 MW/m^2 and strike line widths of up to 11 cm were observed using infrared thermography. The divertor bulk target temperature increased throughout the experimental day, seldomly up to 400 °C [6]. The surface temperature at the strike line could reach temperatures up to 800 °C [23]. The electron temperature in the scrape-off layer was 20 – 100 eV with electron densities of 2 – 6×10^{18} m^{-3} [24, 25].

2.2 PWI samples and sample analysis

Special exchangeable PWI target elements for erosion/deposition investigations at the TDU were developed [9] and exchanged during the opening between OP 1.2a and OP 1.2b. While on most tiles special carbon marker coatings with molybdenum interlayer were used for measuring erosion/deposition of carbon [9], in TDU 1l (lower TDU in module 1) at the strike line position of TM2h6 three tiles with tungsten marker coatings were used. The tungsten coatings were deposited using the CMSII technique [27]. The tungsten layer thicknesses were characterized before exposure in W7-X using ion beam analysis techniques (see below) and had an initial thickness of about 9.2×10^{18} atoms/cm^2 (about 1.5 µm).

Similar marker layers consisting of carbon/molybdenum layers and tungsten layers were used on two scraper elements and exposed during OP 1.2b.

Additionally 21 W-coated fine-grain graphite tiles were exposed at the inner heat shield at various positions. The initial W layer thicknesses were in the range between 5.5×10^{17} and 1.3×10^{18} atoms/cm^2 (about 90 to 200 nm).

All samples were analyzed before and after exposure in W7-X using Elastic Backscattering Spectrometry (EBS) at the IPP tandem accelerator facility in the Bombardino chamber using the BesTec flange [28]. Incident protons with an energy of 2.5 MeV at normal incidence and a scattering angle of 165° were used. A passivated implanted planar silicon (PIPS) detector with a thickness of 300 µm and nominal energy resolution of about 12 keV was used. The measured spectra were analyzed using the program SIMNRA [30] with SRIM [31] stopping powers and non-Rutherford SigmaCalc scattering cross-sections for ^{12}C, ^{13}C and ^{16}O [32]. Surface roughness was taken into account using the simplified model from [33].

Laser-Induced Breakdown Spectroscopy (LIBS) measurements were performed in a vacuum of 10^{-5} Pa using a laser pulse length of 35 ps and a pulse energy of 18 mJ with a repetition rate of 10 Hz at a wave length of 355 nm [34]. The laser beam spot diameter was 0.7 mm. The plasma emission was observed with an optical fibre and collected by a compact Czerny-Turner spectrometer from Ocean Optics in the wavelength range from 350 to 800 nm with a resolution of about 0.2 nm/pixel. This wavelength range covers lines of hydrogen and of B, C, N, O, and Mo.

Scanning electron microscopy (SEM) was performed with a FEI Helios nanolab 600 with focused ion beam (FIB) for cross-sectioning and energy dispersive X-ray spectroscopy (EDX) capabilities from Oxford Instruments Ltd. SEM images were recorded with 5 keV incident electrons. Samples were tilted by 52° for recording FIB cross-sections.

3. Results and discussion

3.1 Test Divertor Unit (TDU)

A schematic representation of the TDU is shown in Fig. 1 (top) together with a scraper element. The TDU consists of a horizontal and a vertical module, the pumping gap is in between. Three W-coated tiles were exposed at position TM2h6 close to the pumping gap, see Fig. 1 (bottom). Only the Standard configuration had its strike line on the W-coated tiles, while the Low Iota configuration has the strike line on the carbon-coated tile 004 and the High Iota and High Mirror configurations have their strike lines on different parts of the TDU [6].

The three W-coated tiles are shown in detail in Figs. 2 and 3. LIBS measurements of the W signal are shown in Fig. 2. The depth scale shown on the left hand side is calibrated for tungsten (ablation rate 30 nm/pulse), but not for the deposits on top of the W layers. W light emission is observed already at the very surface in the range 10 to 40 mm and around 190 mm, i.e., at these areas the W marker layer is still at the very surface. At all other areas the W light emission begins only after a few laser pulses, i.e., here the W layer is coated with a different material. The W light emission is less pronounced in the area from 110 to 170 mm, i.e., in this region the total amount of W is smaller and some W has been eroded.

The W layer thicknesses and the differences of W layer thickness before and after exposure, as determined by EBS, are shown in Fig. 3(b) and 3(c). The accuracy for the determination of the amount of W is about 5%. Erosion of W is clearly seen at positions between 115 and 215 mm, the maximum erosion of about 4×10^{18} atoms/cm^2 (about 630 nm) is observed around 135 mm. Between 15 and 115 mm the amount of tungsten after exposure is identical within the achieved experimental accuracy to the amount of W before exposure, i.e., here erosion is not observed. Deposition of W is not expected due to the very small amounts of W present in the machine. Taking the maximum observed net tungsten erosion and the total discharge time in Standard configuration during OP 1.2b yields the maximum tungsten erosion rate during Standard configuration discharges of about 8.3×10^{14} atoms/cm^{2}s (about 0.13 nm/s). The probability for prompt redeposition of eroded W depends on position and plasma conditions and reaches maximum values of about 60% [35, section 9.3.3]. Prompt redeposition takes place typically within a few mm from the point of origin of the sputtered W atom, i.e., W atoms eroded from the W

marker stripe and redeposited by prompt redeposition are usually redeposited again on the marker stripe. The observed net erosion therefore already includes prompt redeposition.

The deposition of B, C and O, as determined by EBS, is shown in Fig. 3(d).The black stripes visible at around 90 mm and around 155 mm are not caused by erosion, but are due to redeposited layers with mean thicknesses up to about 6×10^{18} atoms/cm^2 (about 600 nm) B+C+O. These layers consist mostly of carbon, but contain about 15-20 at% B and about the same amount of O. Small traces of medium-Z elements (Fe, Cr, Ni) could be sometimes identified, but not quantified. Hydrogen cannot be detected by EBS, but can be determined by LIBS and Laser-Induced Ablation-Quadrupole Mass Spectrometry (LIA-QMS) measurements [36]. LIBS depth profiles (not shown) indicate hydrogen to be contained mainly in the redeposited B+C+O layers, while only small amounts of H are trapped in the W layer. The integrated hydrogen LIBS signal, normalized to 1 at the maximum, is shown in Fig. 3(e). The highest amounts of H are observed in areas with codeposited B+C+O layers. The H concentration in the thickest deposits around 90 mm is smaller than in the range from 110 to 160 mm, probably due to higher surface temperatures at the strike line.

FIB cross-sections through the W marker layer are shown in Fig. 4. Erosion/deposition effects are very small at position 1, so that the layer at this position can be considered as almost virgin. The fine-grain graphite surface is rough on a coarse scale due to grinding grooves and on a finer scale due to the graphite grains. The W marker layer follows this rough carbon surface, its thickness is (with some smaller variations) more or less constant measured parallel to the local surface normal. Position 2 is in the maximum of deposition, see Figs. 2 and 3. The W marker layer has not been eroded at this position, but has been covered by a layer consisting of B, C and O. This layer contains also hydrogen. The redeposited layer fills predominantly the valleys of the rough surface, resulting in some smoothing of the initially rough surface. The surface of the redeposited layer has a prominent micro-roughness with a different visual appearance than the original micro-roughness shown at position 1. Position 3 is in the tungsten erosion maximum. The W-layer got visibly thinner at the plasma-inclined ridges and hilltops of the rough surface, while the valleys are net deposition areas of carbon mixed with B and O. This explains the observation of simultaneous erosion and deposition in this area, see Figs. 2 and 3. On the long term this simultaneous erosion of hills and deposition in valleys results in a smoothing of the initially rough surface, as has been already observed with carbon marker layers [9] where the net erosion was much larger and this smoothing effect therefore was more pronounced. Position 4 shows some tungsten erosion and only little deposition. Here the W-layer also got thinner at plasma-inclined ridges and hilltops of the rough surface resulting in net tungsten erosion, see Figs. 2 and 3, while deposition in the valleys is less pronounced than at position 3.

Carbon erosion was not determined in OP 1.2b at TDU 1l due to the W marker layer. Corresponding tiles as the W-coated ones, but with a carbon marker layer, are shown in Fig. 3 right column. These tiles were taken from TDU 5l (lower TDU in module 5), which showed similar carbon erosion within about 20% as TDU 1l in OP 1.2a [9]: These tiles therefore can be taken as rough estimate for the carbon erosion at the position of the W-layers in TDU 1l. The maximum carbon erosion at the strike line is about 5×10^{19} C-atoms/cm^2, which gives a maximum carbon erosion rate at the position of the W marker layer in OP 1.2b of 10^{16} C-atoms/cm^{2}s (about 1 nm/s), i.e., about 13 times larger than the maximum erosion rate of W.

The observed maximum tungsten erosion rate of 0.13 nm/s is comparable within the experimental uncertainties to the tungsten erosion rate observed at the outer strike point of ASDEX Upgrade, where a tungsten erosion rate of > 0.06 nm/s was observed under comparable conditions (W marker layer in a carbon-dominated environment) [37]. With the full-W ASDEX Upgrade an erosion rate of 0.12 nm/s was observed at the outer strike point [38]. At WEST a tungsten erosion rate > 0.1 nm/s was observed at the inner and outer strike points [39]. The ratio of carbon to tungsten erosion rate of 13 is also in line with measurements of the W and C erosion rates at the outer strike point of ASDEX Upgrade, where a ratio of carbon to tungsten erosion of 10 – 20 was observed [37].

It was already concluded earlier that the erosion of tungsten at the divertor under attached plasma conditions is mainly caused by sputtering by light impurities, especially by B, C and O ions [40, 41], while in ELMy H-mode the erosion during ELMs by accelerated fuel- and impurity ions [42] can exceed the erosion in between ELMs considerably [43]. As up to now no ELMs were observed in W7-X, the observed erosion of tungsten at the divertor is due to the attached plasma conditions with relatively high plasma temperatures at the strike line. The observed erosion rates of the W markers are comparable to previous results obtained in the divertor of tokamaks. This shows that the W7-X divertor behaves as expected from tokamak experience. Additional erosion mechanisms, such as erosion by arcs, seem to play only a very minor role at the TDU. It should be kept in mind, however, that up to now the number of samples is very limited and additional erosion mechanisms can be relatively localized. W-erosion at the divertor is expected to be very low for a full W machine if detached plasmas are used and impurity concentrations are kept low.

3.2 Inner heat shield

21 W-coated fine-grain graphite tiles were exposed at the inner heat shield during OP 1.2b at various positions, see Fig. 5. The initial W layer thicknesses were in the range between 5.5×10^{17} and 1.3×10^{18} atoms/cm^2 (about 90 to 200 nm).

A typical result for the thickness distribution of the W marker layer is shown in Fig. 6: The thicknesses of the W marker layer before and after exposure are identical within the experimental uncertainty of about 5%. On all 21 tiles the net W erosion was below the detection limit of 2.5-5x10^{16} W-atoms/cm^2 (about 4 – 8 nm) – the detection limit depends on the initial W layer thickness and is smaller for initially thinner layers. Arc traces or other signs of localized erosion were not observed on the 21 tiles.

After exposure the tiles were relatively homogeneously covered with a thin film consisting mainly of B, C and O – the brownish color of the tile shown in Fig. 6 is due to this film. The thicknesses of the deposits depended on the position inside the machine and were in the range $2\text{x}10^{17} – 10^{18}$ B + C atoms/cm^2. The films typically contained more B than C with B:C ratios in the range 2 – 5 and were most probably deposited during boronizations.

The detection limit discussed above corresponds to a detection limit for the W erosion rate at the inner heat shield of 3 – 6x10^{12} W-atoms/cm^{2}s (about 0.5 – 1 pm/s) – the actual W erosion rate during OP 1.2b was smaller than this upper limit. This is compatible with the low W erosion rate of 0.5 – 2x10^{12} W-atoms/cm^{2}s observed at the inner wall of JET [44], but is somewhat smaller than the W erosion rate of

10^{12} – 10^{13} W-atoms/cm^{2}s at the inner heat shield of ASDEX-Upgrade [45]. The inner heat shield of ASDEX-Upgrade is used as limiter during plasma startup and ramp down, and it was already demonstrated in [45] that the observed tungsten erosion is mainly due to interaction with ions. The inner wall at JET is recessed by several cm behind poloidal inner wall limiters and can be reached only by neutral particles: This explains the lower erosion rate at JET compared to ASDEX-Upgrade. The inner heat shield of W7-X does not show any traces of interactions with ions (i.e., erosion/deposition features with directional characteristics) and is therefore assumed to be hit only by neutral particles created by charge-exchange processes or by very low-energetic ions with energies below the sputtering threshold: This would explain the low W erosion rate.

3.3 Scraper elements

Two scraper elements were coated with Mo/C and W marker layers, see Fig. 7. The initial thicknesses of the W marker layers were about 1.3 µm. The scrapers were mounted close to TDU 3l and 5u and were exposed to 50 successful plasma discharges with a total duration of 237.6 s. The plasma density, as determined by Thomson scattering, was in the range 2–9x10^{19}/m^3. The scraper did not receive significant loads in other scenarios.

The thicknesses of the W marker layers were identical within the experimental uncertainty of about 5% before and after exposure, see Fig. 8. Inhomogeneous deposition of B, C and O was observed on the marker stripes.

4. Conclusions and outlook

A very high carbon erosion rate was observed at the TDU of W7-X during the operational period OP 1.2a [9] due to high oxygen (and subsequent carbon) impurity levels in the plasma [10]. The oxygen impurity level was decreased by 1-2 orders of magnitude by boronizations in OP 1.2b [10], resulting in a decrease of the carbon erosion rate by a factor of more than five in OP 1.2b [10, 13]. Redeposited carbon layers are observed at several places inside the machine, layers at some baffle tiles exceed thicknesses of 10 µm [14] and partly already started to flake off. The still relatively high net carbon erosion even after boronizations and the formation of flaking redeposited carbon layers raises some concern for the future long-pulse operation of W7-X.

A possible solution for the problem of high carbon erosion would be the use of tungsten as plasma-facing material: At detached plasma conditions and low plasma impurity contents the erosion of tungsten by hydrogen ions is extremely small. However, the use of high-Z elements in stellarators is more challenging than in tokamaks due to the higher contribution of neoclassical transport in stellarators, which can result in accumulation of high-Z impurities in the plasma core. The use of high-Z elements in stellarators therefore requires some care.

In order to get first insight into tungsten erosion at the W7-X walls tungsten marker layers were exposed at the TDU strike line, at 21 different positions of the inner heat shield, and at two scraper elements during the operational phase OP 1.2b. The maximum tungsten erosion rate at the TDU strike line was

0.13 nm/s averaged over the whole campaign. The erosion is microscopically inhomogeneous on the rough TDU surface, with higher erosion on the ridges of the rough surface inclined towards the plasma and deposition of mixed carbon layers in the valleys of the rough surface. The W erosion at the inner heat shield was below the detection limit of 3 – 6x10^{12} W-atoms/cm^2s. W-erosion on the scraper elements was also below the detection limit, the marker layers were coated with boron/carbon layers.

Based on these encouraging results the tungsten-coated area at the inner heat shield will be expanded to 2 m^2 in OP 2.1 followed by further expansion of the W-covered areas in the succeeding campaigns. At the baffles 8 pure W and 32 W heavy alloy (W/CuNi) tiles will be installed. The W erosion will be monitored by marker layers and spectroscopy. A W-divertor and a carbon-free device is envisaged for the year 2031 with OP 3.

Acknowledgements

The technical assistance of J. Dorner and M. Fußeder from IPP Garching with the ion beam analysis measurements is gratefully acknowledged. Photographs of all tiles were made by K. Hunger.

This work has been carried out within the framework of the EUROfusion Consortium and has received funding from the Euratom research and training programme 2014-2018 and 2019-2020 under grant agreement No 633053. The views and opinions expressed herein do not necessarily reflect those of the European Commission.

1 Beidler C *et al.* 1990 Physics and Engineering Design for Wendelstein VII-X *Fusion Technol.* **17** 148

2 Wolf RC *et al.* 2017 Major Results from the First Plasma Campaign of the Wendelstein 7-X Stellarator *Nucl. Fusion* **57** 102020

3 Bosch H-S *et al.* 2017 Final Integration, Commissioning and Start of the Wendelstein 7-X Stellarator Operation *Nucl. Fusion* **57** 116015

4 Sunn Pedersen T *et al.* 2017 Key Results from the First Plasma Operation Phase and Outlook for Future Performance in Wendelstein 7-X *Phys. Plasmas* **24** 055503

5 Peacock A *et al.* 2009 Progress in the Design and Development of a Test Divertor (TDU) for the Start of W7-X Operation *Fusion Eng. Des.* **84** 1475

6 Sunn Pedersen T *et al.* 2019 First Results from Divertor Operation in Wendelstein 7-X *Plasma Phys. Controlled Fusion* **61** 014035

7 Sunn Pedersen T *et al.* 2016 Confirmation of the Topology of the Wendelstein 7-X Magnetic Field to Better than 1:100,000 *Nature Communications* **7** 13493

8 Hirsch M *et al.* 2008 Major Results from the Stellarator Wendelstein 7-AS *Plasma Phys. Controlled Fusion* **50** 053001

9 Mayer M *et al.* 2020 Material erosion and deposition on the divertor of W7-X *Phys. Scr.* **T171** 014035

10 Brezinsek S *et al.* Plasma-Surface Interaction in the Stellarator W7-X: Conclusions Drawn from Operation with Graphite Plasma-Facing Components, submitted to *Nucl. Fusion*

11 Sereda S *et al.* 2020 Impact of boronizations on impurity sources and performance in Wendelstein 7-X *Nucl. Fusion* **60** 086007

12 Wang E *et al.* 2020 Impurity sources and fluxes in W7-X: from the plasma-facing components to the edge layer *Phys. Scr.* **T171** 014040

13 Mayer M *et al.* 2021 Material erosion, deposition and transport in the divertor region of W7-X, presented at the PSI 2021

14 Dhard CP *et al.* 2021 Plasma-wall interaction studies in W7-X: Main results from the recent divertor operations, presented at the PFMC 2021

15 Tsitrone E. *et al.* 2009 Deuterium inventory in Tore Supra: reconciling particle balance and post-mortem analysis *Nucl. Fusion* **49** 075011

16 Bolt H *et al.* 2004 Materials for the plasma-facing components of fusion reactors *J. Nucl. Mater.* **329–333** 66

17 Kallenbach A *et al.* 2009 Non-boronized compared with boronized operation of ASDEX Upgrade with full-tungsten plasma facing components *Nuclear Fusion* **49** 045007

18 Matthews GF *et al.* 2011 JET ITER-like wall—overview and experimental programme *Phys. Scr.* **T145** 014001

19 Bucalossi J *et al.* 2014 The WEST project: Testing ITER divertor high heat flux component technology in a steady state tokamak environment *Fusion Eng. Des.* **89** 907

20 Yao DM *et al.* 2016 Design, R&D and commissioning of EAST tungsten divertor *Phys. Scr.* **T167** 014003

21 Burhenn R *et al.* 2009 On impurity handling in high performance stellarator/heliotron plasmas *Nucl. Fusion* **49** 065005

22 Sunn Pedersen T and W7-X Team 2021 Experimental confirmation of efficient island divertor operation and successful neoclassical transport optimization in Wendelstein 7-X, presented at FEC 2021 and submitted *to Nucl. Fusion*

23 Gao Y *et al.* 2019 Methods for Quantitative Study of Divertor Heat Loads on W7-X *Nucl. Fusion* **59** 066007

24 Barbui T *et al.* 2018 The He/Ne beam diagnostic for active emission spectroscopy in the island divertor of Wendelstein 7-X, 45th EPS Conference on Plasma Physics, Prague, Czech Republic, P4.1018

25 Effenberg F *et al.* 2019 Investigation of 3D effects on heat fluxes in performance-optimized island divertor configurations at Wendelstein 7-X *Nucl. Mater. Energy* **18** 262

27 Ruset C *et al.* 2009 Industrial scale 10 µm W coating of CFC tiles for ITER-like Wall Project at JET *Fusion Eng. Des.* **84** 1662

28 Mayer M *et al.* 2020 Ion beam analysis of fusion plasma-facing materials and components: facilities and research challenges *Nucl. Fusion* **60** 025001

30 Mayer M 2014 Improved Physics in SIMNRA 7 *Nucl. Instrum. Methods Phys. Res. B* **332** 176

31 Ziegler JF 2004 SRIM-2003 *Nucl. Instrum. Methods Phys. Res. B* **219–220** 1027

32 Gurbich AF 2016 SigmaCalc Recent Development and Present Status of the Evaluated Cross-Sections for IBA *Nucl. Instrum. Methods Phys. Res. B* **371** 27

33 Mayer M 2002 Ion Beam Analysis of Rough Thin Films *Nucl. Instrum. Methods Phys. Res. B* **194** 177

34 Zhao D *et al.* 2020 Ex-situ Analysis of W7-X Divertor Plasma-facing Components by Picosecond Laser Diagnostics Phys. Scr. **T171** 014018

35 Naujoks D, Plasma-Material Interaction in Controlled Fusion, Vol 39 of Springer Series on Atomic, Optical and Plasma Physics, Springer, Berlin, Heidelberg, New York, 2006

36 Oelmann J *et al.* 2021 Hydrogen content in divertor baffle tiles in Wendelstein 7-X *Nucl. Mater. Energy* **26** 100943

37 Mayer M *et al.* 2007 Erosion of tungsten and carbon markers in the outer divertor of ASDEX-Upgrade *Phys. Scr.* **T128** 106

38 Hakola A *et al.* 2015 Erosion of tungsten and steel in the main chamber of ASDEX Upgrade *J. Nucl. Mater.* **463** 162

39 Balden M *et al.* 2021 Erosion and redeposition patterns on entire erosion marker tiles after exposure in the first operation phase of WEST, presented at PFMC 2021 and submitted to *Phys. Scr.*

40 Thoma A *et al.* 1997 Spectroscopic measurements of tungsten erosion in the ASDEX Upgrade divertor *Plasma Phys. Control. Fusion* **39** 1487

41 Krieger K, Maier H, Neu R and ASDEX Upgrade Team 1999 Conclusions about the use of tungsten in the divertor of ASDEX Upgrade *J. Nucl. Mater.* **266-269** 207

42 Brezinsek S *et al.* 2019 Erosion, screening, and migration of tungsten in the JET divertor *Nucl. Fusion* **59** 096035

43 Dux R *et al.* 2009 Plasma-wall interaction and plasma behaviour in the non-boronised all tungsten ASDEX Upgrade *J. Nucl. Mater.* **390–391** 858

44 Krat S *et al.* 2021 Comparison of JET inner wall erosion in the first three ITER-like wall campaigns, submitted to *Nucl. Mater. Energy*

45 Krieger K, Maier H, Neu R, Rohde V, Tabasso A 2001 Plasma–wall interaction at the ASDEX Upgrade tungsten heat shield *Fusion Eng. Des.* **56–57** 189

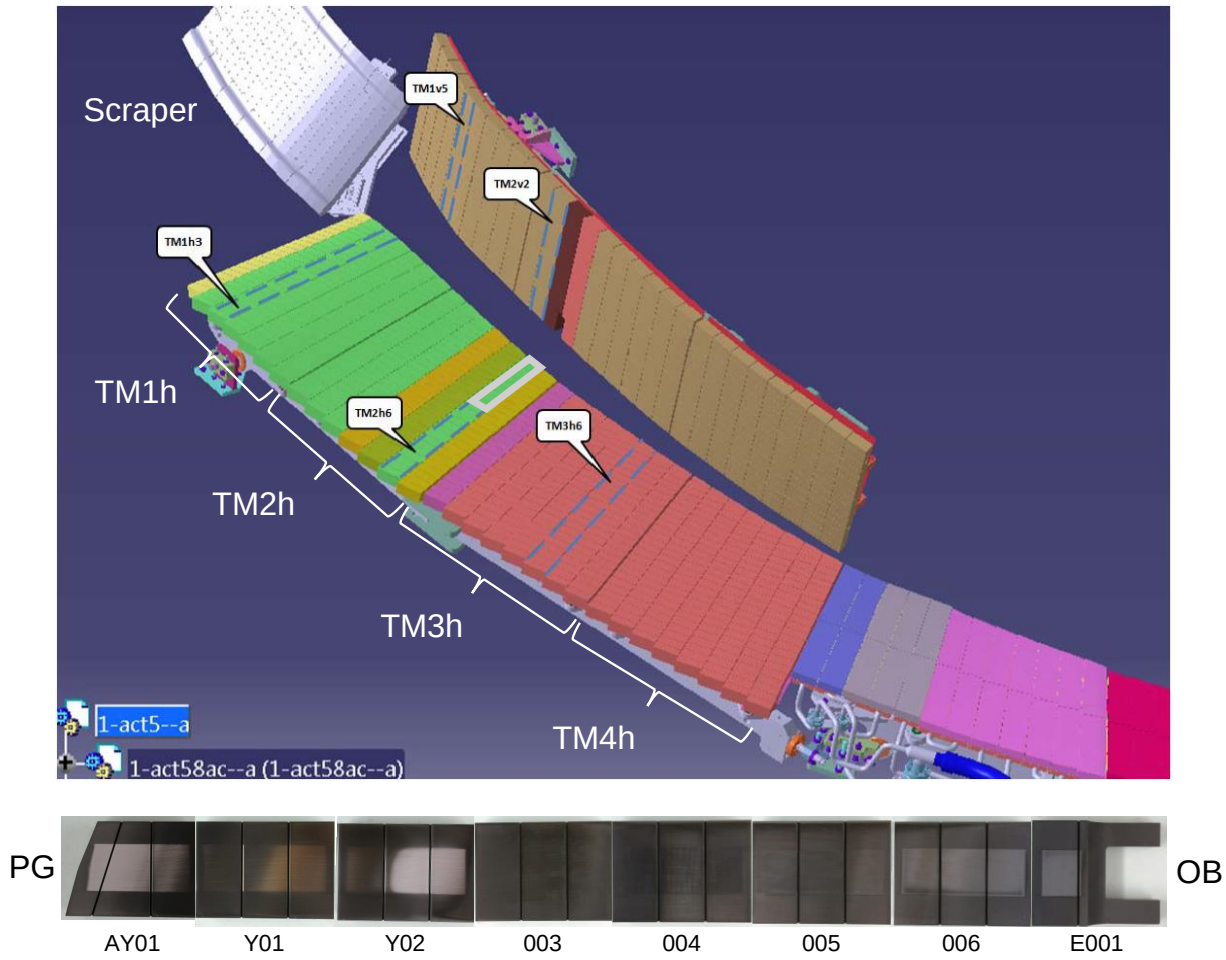

Fig. 1: Top: Schematic representation of the TDU. W-coated tiles were exposed at position TM2h6, the grey rectangle marks the position of the W-coated tiles. Scraper elements were used in OP 1.2b in order to protect the pumping gap between the horizontal and the vertical target. Bottom: Photos of the 8 tiles from TDU 1l position TM2h6 after exposure in OP 1.2b. Tiles AY01, Y01 and Y02 were coated with a tungsten marker layer, tiles 003 to 006 and E001 were coated with Mo/C marker layers. The length of tiles Y01 to 006 is 75 mm each. PG is the direction towards the pumping gap; OB is the direction towards the outer baffle.

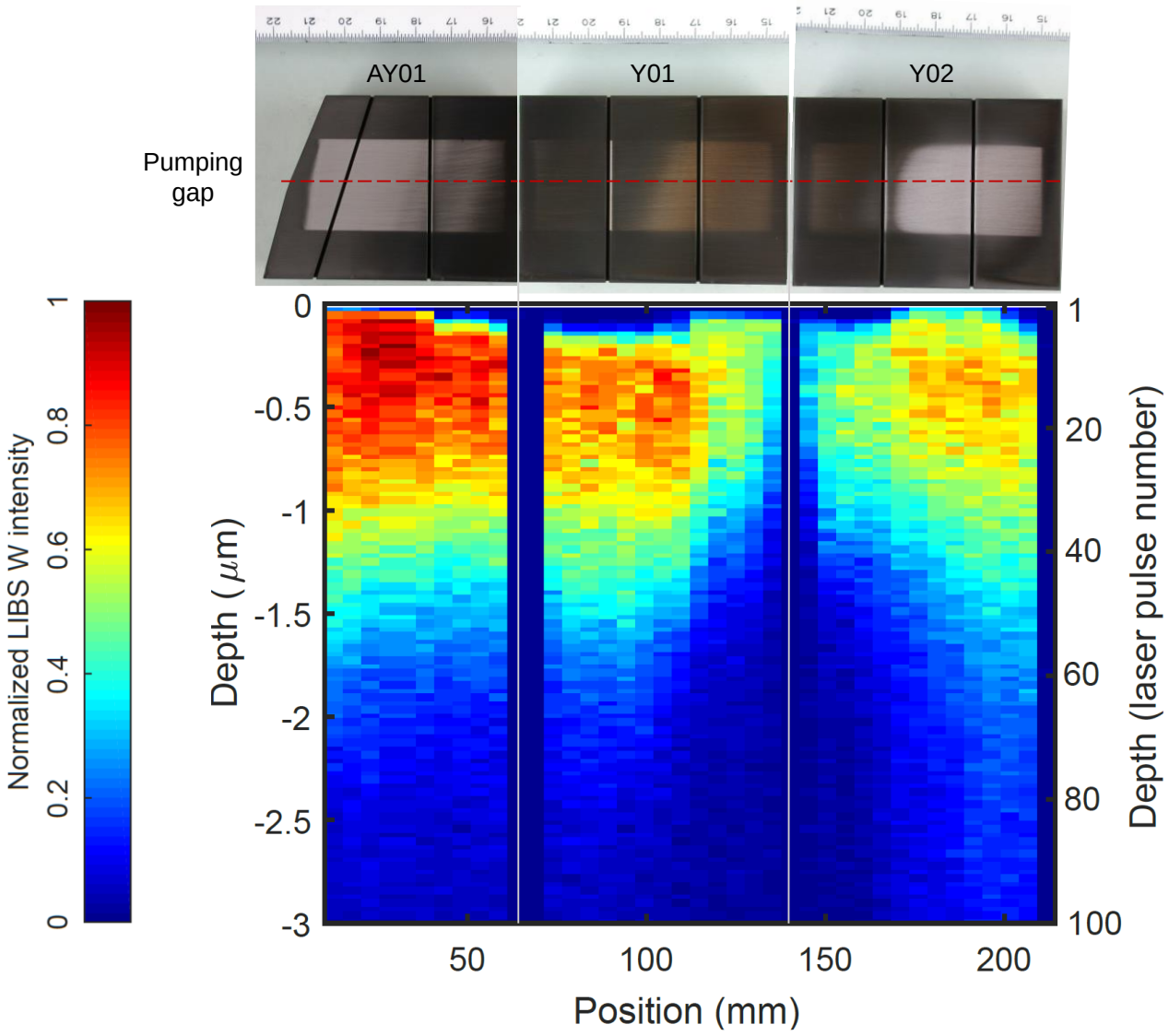

Fig. 2: Top: Photos of the three tungsten-coated tiles after exposure in OP 1.2b. LIBS measurements were made along the red dashed line. Bottom: LIBS intensity of the W I line. The left scale is calibrated for tungsten and assumes an ablation rate of 30 nm per pulse. The right hand scale is given in laser pulse numbers. The origin of the position is at the pumping gap, see also Fig. 3.

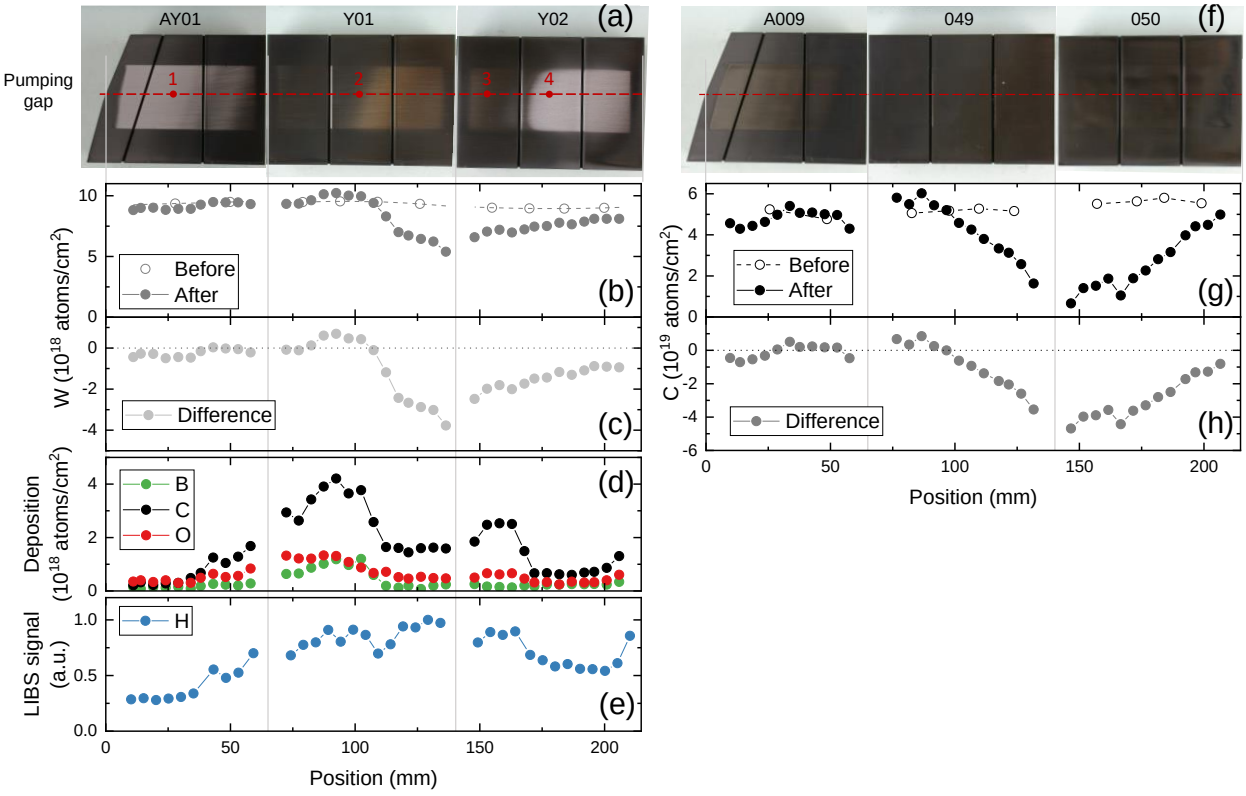

Fig. 3: Left column: W-coated tiles in TDU 1l; right column: C-coated tiles in TDU 5l. (a) Photos of the three tungsten coated tiles after exposure in OP 1.2b. Ion beam analysis measurements were made along the red dashed line. Red dots labeled 1 – 4 are positions for which FIB cross-sections are shown in Fig. 4. (b) Thicknesses of the W marker layers before exposure (grey hollow dots and dashed line) and after exposure (grey filled dots and solid line). (c) Light grey dots and solid line: Change of W layer thickness; a negative sign means erosion. (d) Deposition of B, C, and O. (e) Amount of H, as derived from LIBS. (f) Photos of three carbon marker coated tiles after exposure in OP 1.2b. (g) Thicknesses of the C marker layers before exposure (black hollow dots and dashed line) and after exposure (black filled dots and solid line). (h) Grey dots and solid line: Change of C layer thickness; a negative sign means erosion. Note the different scales for W and C erosion. The origin of the position is at the pumping gap.

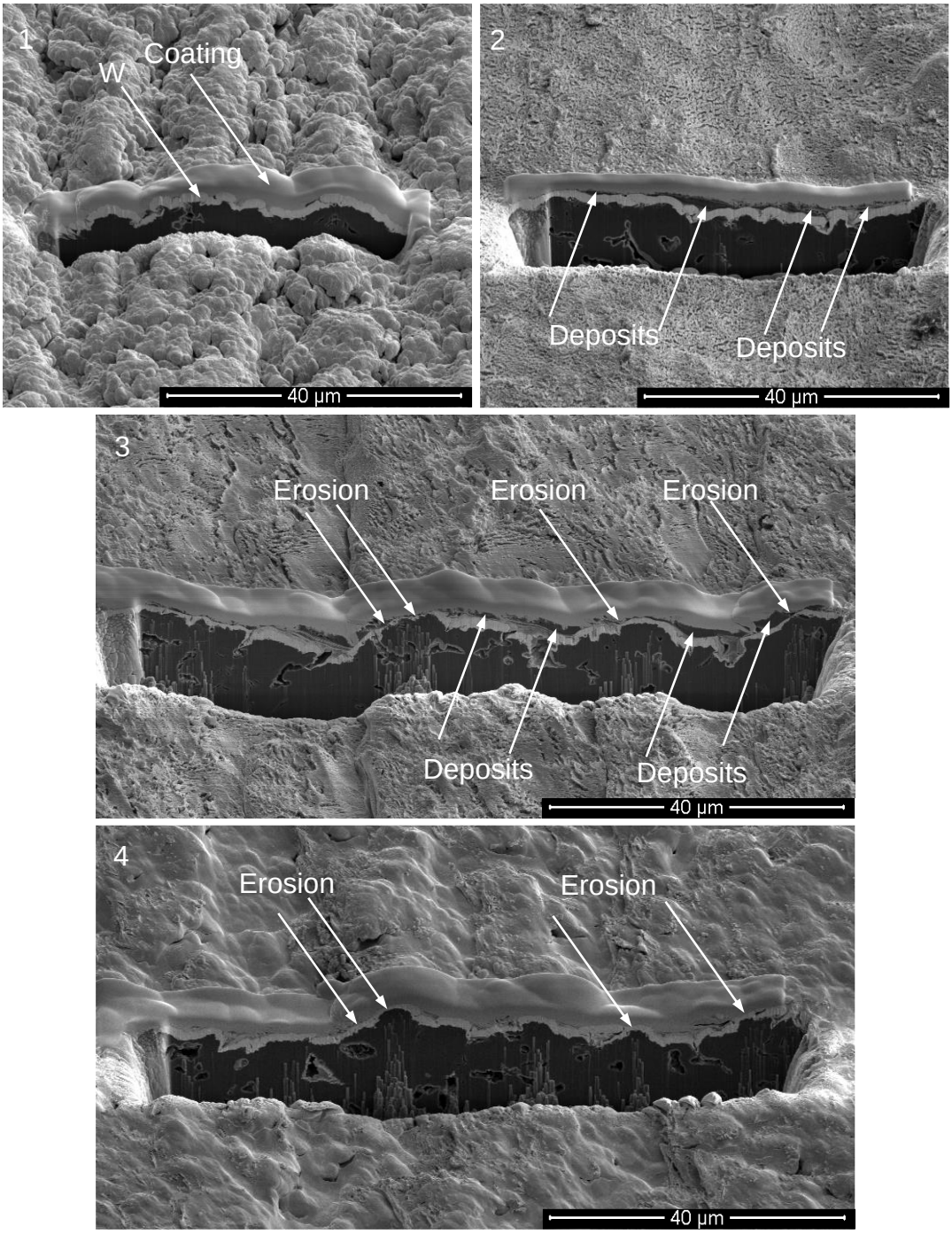

Fig. 4: Focused ion beam cross-sections of the W marker layer after OP 1.2b at positions 1 – 4, see Fig. 3. The images were recorded with secondary electrons, the W marker layer appears as bright band at or close to the surface in the cross-sections (marked as “W” in position 1). The surface was locally coated in-situ with a Pt/C protection layer prior to the cross-sectioning (marked as “Coating” in position 1). Deposits consisting of H, B, C and O (see Fig. 3(d) and 3(e)) on top of the W marker layer are marked as “Deposits”; areas with visible thinning of the W marker layer are marked as “Erosion”.

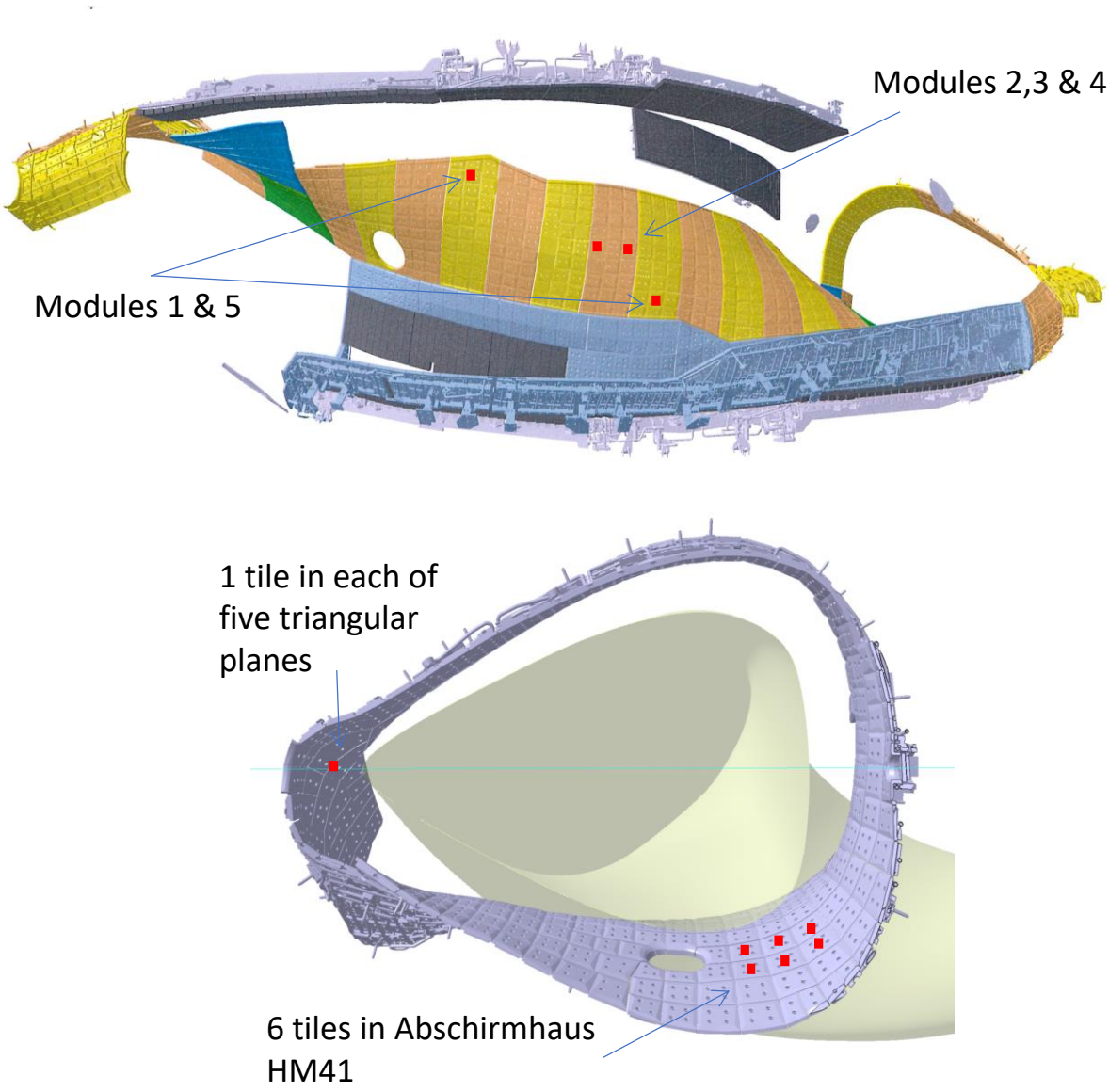

Fig. 5: Positions of the 21 W-coated inner heat shield tiles exposed in OP 1.2b.

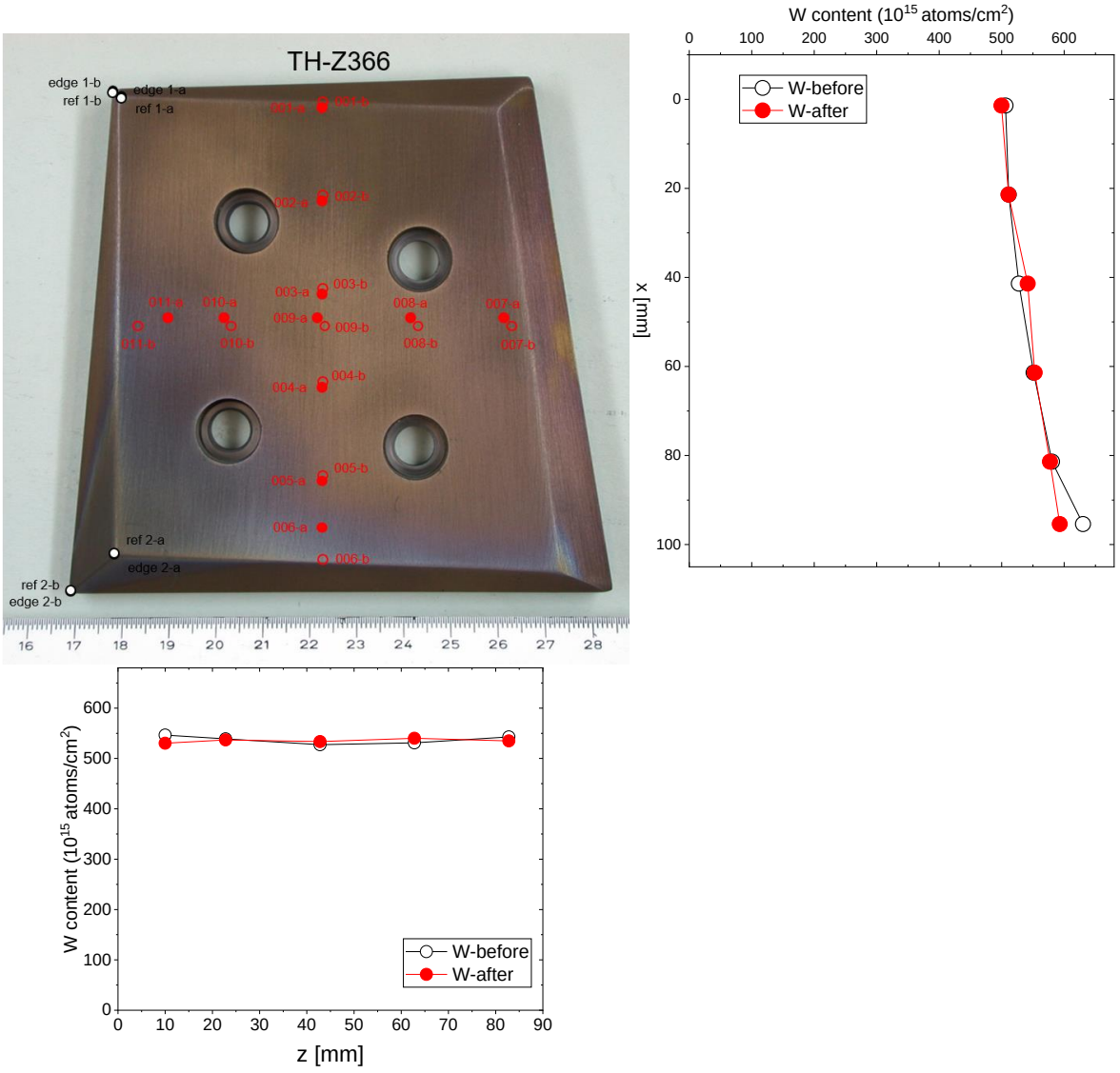

Fig. 6: Photo of tile TH-Z366, exposed in HM22, after exposure during OP 1.2b. Open black dots: Positions of EBS measurements before exposure; Red dots: Positions of EBS measurements after exposure. Graphs: Thicknesses of the W marker layer before (black open dots) and after (red solid dots) exposure in vertical and horizontal direction.

Fig. 7: View of a scraper element inside W7-X. The scraper has a W and a Mo/C marker layer close to the Langmuir probe arrays.

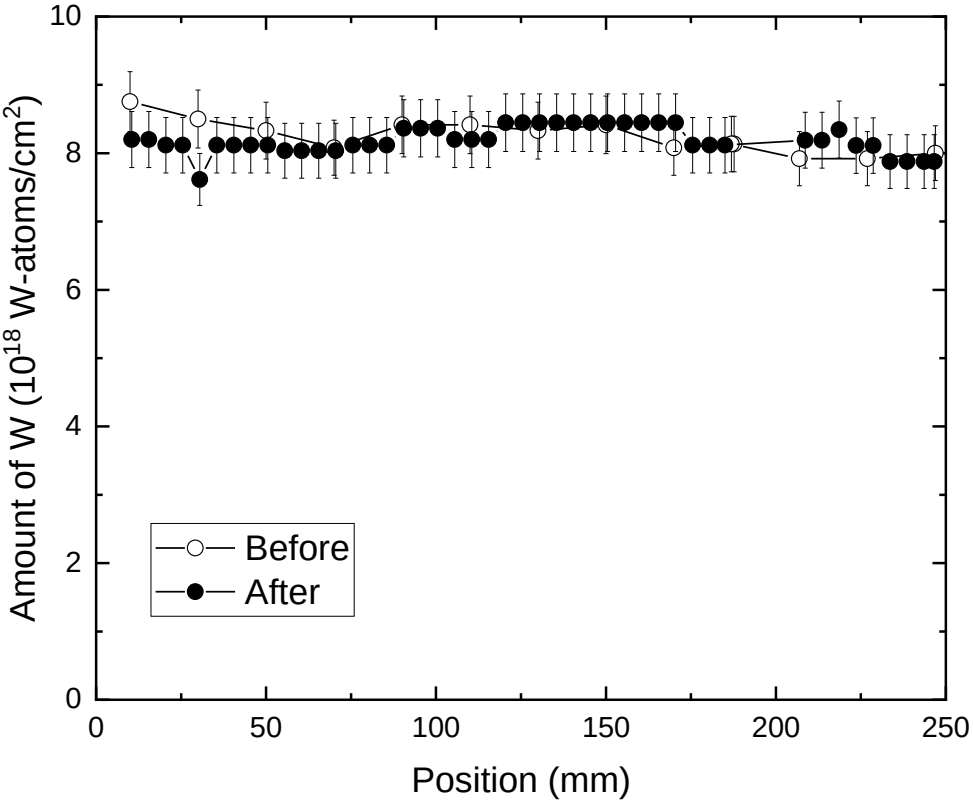

Fig. 8: Thicknesses of the W marker layer at position 207W before (hollow dots) and after (solid dots) exposure in OP 1.2b. The experimental uncertainty in the determination of the amount of W is about 5% and indicated by the error bars.